SLAC–PUB–6358
October 1993
(T/E)

Techniques for the Measurement of Higgs Boson Branching Fractions*

M. D. Hildreth, T. L. Barklow, D. L. Burke

Stanford Linear Accelerator Center
Stanford University, Stanford, California 94309

Abstract

We describe methods that can be employed at a $\sqrt{s} = 500$ GeV e^+e^- linear collider to measure the branching fractions of a Higgs boson. These methods select one Higgs decay mode above all others with high purity, leaving measureable Standard Model backgrounds as the only source of contamination. Integrated luminosities of 50 fb^{-1} are required to obtain statistical errors of 10–20% on the branching fractions to $b\bar{b}$, $\tau^+\tau^-$, and $WW^{(*)}$. For an intermediate-mass Higgs this is sufficient to distinguish the MSSM from the Standard Model Higgs over most of the Supersymmetric parameter space.

Submitted to *Physical Review D*

---

*Work supported by Department of Energy contract DE–AC03–76SF00515

INTRODUCTION

The nature of Electroweak Symmetry Breaking remains as one of the last unexplored frontiers in our understanding of the Electroweak interactions. The standard $SU(2)_L \times U(1)$ model of these interactions [1] predicts a neutral scalar (H^0) called the Higgs particle which breaks the symmetry of the Electroweak interaction and gives mass to the fundamental fermions. Supersymmetric models [2], such as the Minimal Supersymmetric extension to the Standard Model (MSSM), predict a cadre of Higgs particles for the same purpose. Testing these models to truly understand the nature of the Higgs particle will be a crucial experiment if such a particle is discovered at a future colliding-beam facility such as SSC/LHC, NLC, or LEP-II. Since the various models for the Higgs interaction differ in the way the Higgs couples to the known standard model particles, measuring these couplings is a natural and sensitive way to distinguish between the competing theories. Thus, measurements of the branching fractions of the Higgs boson are sensitive probes into the nature of the Higgs couplings. It is generally agreed that an e^+e^- linear collider [3] would be the most powerful experimental setting for establishing a detailed picture of the Higgs boson, as one could exploit the full power of techniques developed for physics analysis at these machines. A center-of-mass energy of 500 GeV or slightly lower is seen as the first stage of the operation of an NLC, with upgrades bringing the available energy to 1 or 1.5 TeV. The lower initial center-of-mass energy is beneficial to studies of intermediate-mass Higgs particles for a number of reasons, including lower backgrounds from other standard model processes and a larger cross section for the reaction $e^+e^- \rightarrow Z^0H^0$ [4]. Here, we present general techniques for measuring the branching fraction of an intermediate-mass Higgs to as many of the standard model particles as possible, assuming the Higgs has already been discovered and that its mass is known with a precision of approximately 5 GeV.

The analyses in this paper focus on an interesting region of Higgs mass, $M_H \leq 2M_W$, where the Higgs can decay to most of the standard model particles with measureable branching fractions. Figure 1(a) shows the branching fractions of the standard model

Higgs boson as a function of its mass. Figure 1(b) gives the branching fractions of the lightest CP-even Higgs in the MSSM as a function of the ratio of the supersymmetric vacuum expectation values $\tan\beta$ [5], where the Higgs mass is chosen to be 120 GeV. Note the difference in the branching fraction to boson pairs for the two cases, especially to W pairs. The branching fraction for this mode is non-negligible even down to Higgs masses of 110 GeV, making it potentially the most useful in distiguishing the Standard Model Higgs from the MSSM Higgs over a large range in $\tan\beta$ for this region of lighter Higgs masses.

We begin with a detailed description of the assumed accelerator parameters, detector simulation, and differential cross sections used in the Monte Carlo programs for this study. We then present the elements of the different analyses used to extract the branching fractions of the Higgs.

ACCELERATOR PARAMETERS

In simulating collision processes at high energy e^+e^- linear colliders, consideration must be given to the interactions between the collective electromagnetic fields of the particle bunches and the beam particles themselves. The beam densities required for sufficient luminosity for particle physics will result in extremely large electromagnetic fields, which can affect the motion of particles involved in the collision. Radiation of photons in the beam-beam collision ("beamstrahlung") will degrade the available center-of-mass energy, resulting in lower luminosity at the design energy of the accelerator [6]. As a result, the amount of beamstrahlung that occurs has become an important parameter in linear collider design. Figures 2(a), (b), and (c) show center of mass energy spectra due to beamstrahlung calculated for three different linear collider designs in the approximation of no intrinsic initial-state radiation. Figure 2(d) shows the center-of-mass energy spectrum from initial state radiation alone. Any annihilation events that occur will have a center-of-mass energy spectrum that is the convolution of initial-state radiation and the beamstrahlung spectrum resulting from the collider design. Initial state radiation and beamstrahlung are comparable

in their degradation of the center-of-mass energy spectrum away from the beam energy. It can also be shown [7] that hard radiation is almost always due to only one of the initial state particles, not both. This allows kinematic fits where the missing momentum along the beam axis and the missing energy are the same. The beamstrahlung spectrum we assume for these analyses, which is calculated assuming the Palmer F accelerator parameters [3], is identical to the spectrum labeled "X-Band" in Fig. 2. Thus, this is a "worst case" estimate of the center-of-mass energy smearing due to beam-beam radiation.

EVENT AND DETECTOR SIMULATION

One of the great advantages of physics experiments at high-energy e^+e^- colliders is that the high-p_T background processes that might obscure a Higgs signal are relatively small in size and are theoretically well-understood and accurately calculable. At these energies, the dominant background cross-sections are due to hard electroweak and QCD processes. Figure 3 shows a plot of the cross section for the processes [8] $e^+e^- \to W^+W^-$ and $e^+e^- \to q\bar{q}$ as functions of center-of-mass energy. At 500 GeV, one unit of R corresponds to 4000 events per year at typical design luminosities. For integrated luminosities of 50 fb^{-1} at center-of-mass energies around 500 GeV, these background processes contribute more than one million events per year to the data volume. It should be emphasized that these standard model processes (and others with much lower cross-sections, such as [9] $e^+e^- \to Z^0Z^0$ and $e^+e^- \to WWZ$) are the *only* significant sources of backgrounds for most physics analyses, including studies of the Higgs.

Table I lists the cross sections (including beamstrahlung and initial-state radiation) and the number of Monte Carlo-generated events for the Higgs decay modes and the background processes considered in this study.

Signal events are generated using the differential cross sections given in Ref. 4. The electroweak backgrounds $e^+e^- \to W^+W^-$ and $e^+e^- \to Z^0Z^0$ are simulated using the formulae given in Refs. 8 and 9 respectively. The cross sections given by Ref. 10 are used to

generate $e^+e^- \rightarrow e\nu W$ events. Top quark pairs are simulated using the work of Ref. 11. The LUND 6.3 model [12] is used to generate the QCD background of five light quark flavors and to fragment and hadronize the decay products of all the events in this study. In order to emphasize that the required detector performance for analyses at a high-energy e^+e^- linear collider are similar to those achieved with current technology, the detector properties used for this study are chosen to be similar to those of the SLD detector [13]. In particular, final state particles are smeared according to Table II. Note that for charged particles, the momentum from the tracking system is always used, as this is far more accurate than the calorimeter for virtually all particles. An overlap-subtraction technique is used to extract the neutral energy where charged-track and neutral clusters overlap in the calorimeter. As can be seen from the table, this results in a degradation of energy resolution for these particles, but the added information on the total energy present markedly improves the overall energy/mass resolution of the detector.

All leptons are considered to be indentified with 100% accuracy, although in reality none of the analyses would be severely affected by the lepton identification efficiencies obtained with existing detectors. In addition, all tracks with p_T less than 150 MeV/c and all particles within 10° of the beamline are removed.

A high-precision vertex detector is used to distinguish those tracks which miss the event origin by an amount significantly larger than the error on the measured distance. We assume that the measurement error on the impact parameter b, the three-dimensional distance-of-closest approach to the interaction point, can be parametrized in the following manner:

$$\sigma_b \cong \sqrt{A^2 + \left[\frac{B}{p\sqrt{\sin^3\theta}}\right]^2}.$$

We have set the asymptotic resolution term A to 5 μm in the plane perpendicular to the beam axis, and to 20 μm along the beam axis. The multiple-scattering term B has been chosen to be 50 μm in both cases. These resolutions are comparable to those obtained by the SLD collaboration with a CCD pixel vertex detector [14].

One identifies events containing heavy quarks by counting the number of tracks having large values of $b_{\rm norm} = b/\sigma_b$. Table III shows that this method can be used to distinguish and accept $H \to WW^{(*)}$ events while rejecting $H \to b\bar{b}$ events with high efficiency. This can be seen graphically in Fig. 4, which shows the distributions of the number of high impact parameter tracks with significance greater than 3 per event for several different Higgs decay modes. Note that, as would be expected, the distribution for $H \to b\bar{b}$ has a rather long tail due to the long lifetime of the b quark. Since the tracks from $H \to WW^{(*)}$ and $H \to gg$ come predominantly from light quarks, these distributions peak at zero tracks, while the distribution for $H \to c\bar{c}$ peaks somewhere between. This may prove to be a useful tool in distinguishing $H \to c\bar{c}$ events from the other events containing light quarks, and hence measuring the branching fraction for $H \to c\bar{c}$.

MEASUREMENT OF HIGGS BRANCHING FRACTIONS

If a Higgs boson is discovered at a future accelerator, it will be imperative to learn as much as possible about the Higgs so as to understand the true nature of electroweak symmetry breaking. Besides its mass, the parameters which determine the relationship of the Higgs to the standard model are its couplings to the standard model particles. This presents the experimenter with a series of measureable constants:

Vector Boson Couplings

These can be determined by measuring the total cross-section for the Bjorken bremsstrahlung process $e^+e^- \to Z^0H^0$, or by measuring the branching fractions for $H \to WW^{(*)}$ and $H \to ZZ^{(*)}$ if the mass of the Higgs is large enough. Note that, since one measures the total cross section times the branching fraction, a measurement of the rate into the $ZZ^{(*)}$ final state would give the absolute width $\Gamma(H \to ZZ^{(*)})$.

Higgs-Fermion Couplings

These can be determined for light fermions by measuring the branching fractions for $H \to b\bar{b}$, $H \to c\bar{c}$, and $H \to \tau^+\tau^-$. The coupling between the Higgs and the top can be

derived by measuring the total cross-section for ttH bremsstrahlung [15], or by measuring the branching fraction for $H \to gg$.

The following subsections present methods for measuring the product $\sigma(e^+e^- \to Z^0H^0)_{tot} \times \Gamma(H \to X\bar{X})$, where X represents any possible final-state particle.

Measurement of $\Gamma(H \to WW^{(*)})$

We present two complementary analyses to measure the branching fraction of the Higgs into W-bosons: one using the hadronic decay modes of both Ws, the second requiring one of the Ws to decay leptonically.

Hadronic Decay Modes (6-jet Analysis)

This analysis requires the reconstruction of the 6-jet final state containing the four jets from the Higgs and the two from the Z, and thus could be applied equally well to study the branching fraction for $H \to ZZ^{(*)}$. Since measurement of the jet-pair masses is crucial, cuts on visible energy ($E_{\rm vis} > 0.8\ E_{\rm CM}$) and total longitudinal and transverse momentum ($\Sigma p_{\rm T} < 20$ GeV, $\Sigma p_z < 30$ GeV) are placed on the events to limit the amount of missing energy taken away by neutrinos or radiation. A containment cut of $\mid \cos\theta_{Thrust} \mid < 0.7$ is also imposed. The event is broken up into 6 jets, and the masses of all possible pairings are computed. The pair closest to the mass of the Z is designated the Z candidate, and the event is rejected if this mass is not within 10 GeV of m_Z. The mass of the other four jets is required to be within 10 GeV of the known Higgs mass. To further reject background, the angle between the two jets from the Z is required to be less than 90°, and the angle between the two jets that comprise the real W from the higgs decay is required to be less than 120°. Once the event has been selected for the ZH final state, several cuts are applied to select specifically for the 6-jet final state where the Higgs decays to 4 jets. The first of these, which generally removes events with a 4-jet final state, is to require that the $y_{\rm cut}$ for the 6-jet solution returned from the JADE cluster-finding algorithm [16] is greater than

8×10^{-4}. This cut is based on the knowledge that, due to the large masses of the Z and Higgs, jets tend to be well-separated in the final state. This is true even if the Higgs decays to a boson virtual-boson pair (a three-body decay), since the invariant mass spectrum of the virtual boson decay products is peaked towards the maximum value allowed kinematically [17]. If the Higgs decays to two fermions, the two jets are usually distinct, and the entire event clearly has four jets. For this event to be constrained into a 6-jet solution, two of the jets have to be split, leaving the largest allowed combination of invariant masses where 6 jets still exist as a relatively small fraction of the total visible energy, and hence a small value of $y_{\rm cut}$. The distribution of $y_{\rm cut}$ values for the 6-jet solution in $H \rightarrow WW^{(*)}$ and $H \rightarrow b\bar{b}$ events is shown in Fig. 5. To remove the background Higgs decay mode with the largest expected rate, an anti-B tag is applied, requiring that there be 3 or fewer tracks with significant large impact parameters ($b_{\rm norm} > 3$) per event.

The signal events then contain 4 jets coming from the Higgs, two of which combine to a mass near m_W, with the other two resulting in an invariant mass lower than the kinematic limit of about 60 GeV for a Higgs mass of 140 GeV. Figure 6(a) shows the mass combinations for the pairings of the 4 jets (signal events only), where the one identified as the W is the pair with a mass closest to m_W. Figure 6(b) shows the results of the analysis. The events counted as lying within the signal region are those in which two jets have masses within 10 GeV of m_W, and the $f\bar{f}$ pair has a mass between 20 and 60 GeV. Assuming Standard Model Higgs couplings, this analysis gives a signal of 17.7 events over a background of 39.4 events. Final results are summarized in Table IV. The background is mostly due to QCD events with good energy balance and many jets and to W pairs.

Leptonic Decay Modes (Missing Momentum Analysis)

This analysis takes advantage of the large branching fraction for the W to decay to leptons, and thus has completely different systematics from the method described above. The strategy is to choose events with one high-momentum, isolated lepton, and then fit

for the missing momentum carried off by the neutrino. Events are selected to contain one and only one lepton of momentum greater than 15 GeV/c plus 4 jets, with the jet pair closest to m_Z being denoted the Z. A cut of $|\cos\theta_{Thrust}| < 0.7$ is used to make certain the event is well contained in the detector. Requiring the p_T of the lepton with respect to the nearest jet to be greater than 5 GeV and that the missing momentum direction have $|\cos\theta_{pmiss}| < 0.983$ removes background events from heavy quark decays and $e^+e^- \rightarrow Z^0Z^0$ events where one of the Z^0s decays into two leptons and one is lost. A cut of 90° on the angle between the two hadronic systems of the Z and the $W^{(*)}$ removes $e^+e^- \rightarrow W^+W^-$ events, since only one of the Ws can decay hadronically. This places the required 4 jets very close together in the final state. In addition, an anti-B tag that requires fewer than 3 tracks with $b_{\rm norm} > 3$ is applied to remove any residual $t\bar{t}$ events. Events which satisfy these cuts are then subject to a 0-C fit with the following constraints: that the visible energy equal the beam energy ($E_{\rm vis} = 2\ E_{\rm beam}$), that the total momentum in all directions be zero ($\Sigma p_x = \Sigma p_y = \Sigma p_z + p_{\rm ISR} = 0$), and that the invariant mass obtained from the fit be equal to the Higgs mass. For more accurate energies to input to the fit, the energy of the Z is rescaled so that $E_Z = \gamma_{\rm obs} m_Z$, where $\gamma_{\rm obs}$ is calculated from the measured β_Z. The varibles of the fit are the three components of the neutrino momentum $p_{\nu x}, p_{\nu y}$, and $p_{\nu z}$, the momentum of the initial-state radiation photon $p_{\rm ISR}$, and the energy of the hadronic W or W^* system $E_{W^{(*)}}$. Figure 7 shows the resulting distribution of the invariant mass from the fitted neutrino momentum and that of the isolated lepton, where the additional requirement that the χ^2 of the 0-C fit be less than 20 has been imposed. The signal region is within 20 GeV of the peak at m_W. Assuming Standard Model couplings for the Higgs, the number of $H \rightarrow WW^*$ events in the signal region around the peak at m_W is 24.3 over a background of 62.2 events. As one can see from the plot, the signal in this mode is marginal. Most of the background in this case comes from W pair events that have enough visible energy from a single W decay to make four jets. This analysis in particular would benefit from improved calorimeter resolution, as the visible partons are reconstructed without the aid of beam-energy constraints.

Measurement of $\Gamma(H \to b\bar{b})$ or $\Gamma(H \to c\bar{c} + gg)$

This analysis takes advantage of the 4-jet nature of $H \to b\bar{b}$ or $H \to c\bar{c}$ and $H \to gg$ events to exclude the Higgs decays to vector bosons. Either a B-tag or anti-B-tag is then applied to select events with b or light quarks, respectively. The event selection cuts are in most cases identical to those for the 6-jet $H \to WW^*$ final state analysis presented above, with several exceptions. Here, 4 jets are required in the final state, and the jet energies are rescaled, keeping the jet angles and velocities fixed [18]. In addition, once the two jets that comprise the Z are identified, the maximum $y_{\rm cut}$ for the Higgs portion of the event to contain 3-jets is computed, and required to be less than 1.8×10^{-2}. This rejects the $H \to VV^*$ events, which tend to have at least 3 jets from the decays of the vector bosons. A B-tag requiring 3 or more tracks with $b_{\rm norm} > 3$, or an anti-B-tag requiring less than 3 tracks with $b_{\rm norm} > 3$ is imposed to select events with b or light quarks, respectively.

The results of this analysis for $H \to b\bar{b}$ events are shown in Fig. 8(a), which shows a signal of 116.8 events over a background of 109.2 events within 20 GeV of the Higgs mass. Most of the background is from W pairs and QCD four-jet events with some long-lived particles that would pass the B-tag. Figure 8(b) shows the acceptance of this analysis with the anti-B-tag applied for the different Standard Model decay modes of the Higgs. Note that the acceptance for the light quark and gluon modes is quite large compared to any other modes. This method will almost certainly be used to isolate a relatively pure sample of light quark events, and thus extract an exclusive measurement of the branching fraction for $H \to c\bar{c}$ events.

Measurement of $\Gamma(H \to \tau^+\tau^-)$

This analysis is similar to that of Ref. 19. Since the Higgs is so much more massive than the τ, the taus in the $H \to \tau^+\tau^-$ decay receive a tremendous boost. Thus, to a good approximation, the decay products of the tau fall into a very narrow cone along its initial

direction. Since the center-of-mass energy and momentum is known, we can reconstruct the initial τ energies and the recoiling Z. At this stage, it is not neccessary to use our (assumed) knowledge of the Higgs mass except to provide initial values for the fit. We only consider here the 1-prong decay modes of the τ for simplicity. The events are required to have some missing energy ($E_{\rm vis} < 0.8\ E_{\rm CM}$), to be contained within the detector ($|\ \cos\theta_{\rm Thrust}\ | < 0.7$), and to have a minimum of 10 charged particles to eliminate background from $e^+e^- \rightarrow Z^0Z^0$ events. Candidates for the two tau decay products are chosen by selecting the two most isolated particles in the event, where isolation ρ is defined by $\rho_i = \min\sqrt{E_i(1 - cos\theta_{ij})}$. The minimum allowed momentum of the two tracks is 5 GeV. These particles must be less than 120° apart, and have opposite charges. In addition, when these particles plus any associated neutrals within a cone of 10° around the particle direction are subtracted from the event the remainder must have a mass within 10 GeV of the Z mass. The final kinematic requirement is that they lie within 11.5° of the plane containing the Higgs (Z) momentum.

The energies of the taus and the recoiling Z are then extracted from a 0-C fit subject to energy and momentum constraints. Figure 9 shows the combined invariant mass of the two taus after their energies have been extracted from the fit. Note that this particular analysis results in extremely low background contamination to the $H \rightarrow \tau^+\tau^-$ sample. The background here is almost entirely due to $e^+e^- \rightarrow Z^0Z^0$ events where the one $Z^0 \rightarrow \tau^+\tau^-$ decay has been badly reconstructed. There are 17.4 signal events over a background of 3 events within 15 GeV of the Higgs mass.

SUMMARY AND CONCLUSIONS

Table IV contains a numerical compilation of the results for the measurements of the Higgs branching fractions presented in the above section. For each analysis the "signal" region used is the one defined in the above descriptions. To calculate the signal-to-noise ratios for each analysis, the Standard Model branching fractions were assumed for a Higgs with mass 140 GeV. The assumed integrated luminosity is 50 $\rm fb^{-1}$. Figure 10(a) shows the

expected errors for the measurements of the branching fractions for the Standard Model Higgs boson. Figure 10(b) shows the expected errors on the Standard Model branching fractions compared to the branching fractions predicted for a 120 GeV *CP*-even MSSM Higgs. The numerical results are summarized in Table V.

As can be seen from these calculations, many of the Standard Model decay modes of the Higgs are accessible to experimental consideration. It is possible to obtain detailed measurements of the Higgs-fermion and Higgs-boson couplings with approximately one year of running at peak luminosity, even with these relatively simple analyses. In fact, most of the measurements have on the order of 20% errors. The one exception is the measurement of the branching fraction for $H \to c\bar{c} + H \to gg$, which can only be used to give an upper limit at this time. More complicated analyses will be neccessary to extract independent measurements of these two branching fractions. However, note the vast difference in the expected branching fraction for $H \to WW^*$ between the Standard Model and the MSSM case, as shown in Fig. 1(b). Since this decay is dominant for a Standard Model Higgs of mass greater than 140 GeV, yet still has a branching fraction of 10% down to a mass of 120 GeV (see Fig. 1(a)), a measurement of this branching fraction should prove to be a powerful discriminatory tool to understand the nature of a discovered Higgs particle.

SUMMARY AND CONCLUSIONS

We would like to thank M. Peskin and H. Haber for many useful discussions. This work was supported by Department of Energy contract DE–AC03–76SF00515.

REFERENCES

[1] S.L. Glashow, Nucl. Phys. B22 (1961) 579; S. Weinberg, Phys. Rev. Lett. 19 (1967) 1264; A. Salam, Proc. 8th Nobel Symposium, Stockholm 1968, ed. N. Svarthholm (Almquist and Wiksells, Stockholm, 1968) p.367.

[2] E. Witten, Nucl. Phys. B188 (1981) 513; S. Dimopoulos and H. Georgi, Nucl. Phys. B193 (1981) 150; N. Sakai, Z. Phys. C11 (1981) 153.

[3] For a review of the design paramters for linear colliders (present and future) see R.B. Palmer, Annu. Rev. Nucl. Part. Sci. 40 (1990) 529 and references within.

[4] J. Gunion, P. Kalyniak, M. Soldate, and P. Galison, Phys. Rev. D 34, 101, (1986).

[5] This Figure and Figure 11 were produced using the results of calculations by H. Haber and R. Hempfling (H. Haber, private communication).

[6] K. Yokoya, Nucl. Instrum. Methods A251, 1 (1986); P. Chen, SLAC–PUB–4293, 1987 (unpublished).

[7] T.L. Barklow, P. Chen, W.L. Kozanecki, "Beamstrahlung Spectra in Next Generation Linear Colliders," in e^+e^- *Collisions at 500 GeV: The Physics Potential*, DESY 92–123, ed. P. Zerwas, p. 845; SLAC–PUB–7063 (unpublished).

[8] R. Philippe, Phys. Rev. D26, 1588 (1982).

[9] R. Brown and K. Mikaelian, Phys. Rev. D19, 922 (1979).

[10] E. Gabrielli, Report No. ROME–550–1987 (unpublished).

[11] S. Komamiya, "Possible Experimental Studies of the $t\bar{t}$ Threshold Region at a 250–500 GeV e^+e^- Collider," Snowmass '90, Ed. E. Berger, p.459.

[12] T. Sjostrand and M. Bengtsson, Comput. Phys. Commun. 43, 367 (1987).

[13] K. Abe *et al.*, Phys. Rev. Lett. 70, 2515 (1993), and references contained therein.

[14] D. Su, "A Preliminary Measurement of R_b at SLD," presented at D.P.F., Dallas, 1992.

[15] A. Djouadi, J. Kalinowski, and P. Zerwas, Z. Phys. C54 (1992) 255.

[16] JADE Collab., W. Bartel *et al.*, Z. Phys. C33 (1986) 23.

[17] W.Y. Keung and W.J. Marciano, Phys. Rev. D30 (1984) 248.

[18] Tasso Collab., M. Althoff, *et al.*, Phys. Lett. B122 (1983) 95.

[19] P. Janot, "Light Higgs Spectrum from e^+e^- Annihilation," proceedings of Electroweak Symmetry Breaking at Colliding-Beam Facilities," Santa Cruz, CA, December 11–12, 1992.

FIGURES

FIG. 1. (a) Branching fractions of the Standard Model Higgs boson as a function of its mass for a 150 GeV top quark mass. (b) Branching fractions of the lightest CP-even Higgs in the MSSM as a function of $\tan\beta$, for a top quark mass of 175 GeV. An explanation of plot symbols is given above the plot.

FIG. 2. Center of mass energy spectra from beamstrahlung only for several linear collider designs. The curves come from designs for colliders with a linac based on: (a) X-Band RF; (b) S-Band RF; (c) Superconducting RF. For comparison, (d) shows the center of mass energy spectrum from initial state radiation only.

FIG. 3. Production cross-sections for the dominant Standard Model processes at high energy.

FIG. 4. The distributions of number of tracks with impact parameter significance greater than 3 for several Higgs decay modes. The plots show purely the expected shapes of the distributions; no assumptions on branching fractions have been made.

FIG. 5. Distributions for the maximum allowable y_{cut} value such that the event contains 6 jets, shown for typical 4-jet events ($H \to b\bar{b}$) and typical 6-jet events ($H \to WW^{(*)}$). The arrow shows where the cut was placed. Note the log scale of the vertical axis.

FIG. 6. (a) The distribution of jet masses within the 4 jets from the Higgs decay. Note that the mass of the $f\bar{f}$ pair from the W^* follow the distribution expected from the kinematics of this decay. (b) Final results of the analysis, after all cuts. A signal of $H \to WW^*$ events represented by the reconstructed W^* can be seen clearly above 50 fb^{-1} of background. The number of signal events assumes the branching fractions for a Standard Model Higgs.

FIG. 7. The resulting fit lepton-neutrino mass for $H \to WW^*$ events over 50 fb^{-1} of background events. The number of signal events is normalized assuming Standard Model branching fractions for the Higgs.

FIG. 8. (a) Results of the 4-jet analysis with B-tagging applied to isolate events containing b quarks. An integrated luminosity of 50 fb^{-1} and Standard Model branching fractions for the Higgs are assumed. (b) Acceptance in percent of this analysis for events containing lighter quarks, where an anti-B-tag has been applied.

FIG. 9. Mass distribution of the tau pairs reconstructed by a kinematic fit assuming a recoiling Z opposite two particles. See text for a more detailed description. The Standard Model branching fractions for the Higgs have been assumed to make this plot.

FIG. 10. (a) Expected errors on the measurement of the Standard Model branching fractions for a Higgs mass of 140 GeV. The points have been displaced slightly to allow the error bars to be seen. This plot assumes an integrated luminosity of 50 fb^{-1} and Standard Model couplings for the Higgs. (b) Expected errors on the Standard Model branching fractions with the predicted branching fractions for a 120 GeV CP-even MSSM Higgs.

TABLES

TABLE I. A summary of the cross sections and generated events for this study.

	$\sigma(pb)$ (with beamstrahlung)	events ($50\ \mathrm{fb}^{-1}$)	simulated
Signal events:			
$H \to b\bar{b}$	0.044	2200	10,000
$H \to WW^*$	0.055	2750	10,000
$H \to ZZ^*$	0.007	350	5,000
$H \to c\bar{c}$	0.0025	125	5,000
$H \to gg$	0.004	200	5,000
$H \to \tau^+\tau^-$	0.004	200	5,000
Backgrounds:			
$e^+e^- \to W^+W^-$	9.9	495,00	43,997
		0	
$e^+e^- \to q\bar{q}$	16.1	805,00	46,935
		0	
$e^+e^- \to t\bar{t}$	~ 1.0	50,000	7,500
$e^+e^- \to Z^0Z^0$	0.59	29,500	12,787
$e^+e^- \to e\nu W$	3.6	180,000	32,374
		0	

TABLE II. Resolutions used in the smearing of final-state particles for these analyses.

Particle Type		Detector Resolution
charged tracks		$\sigma(p) = 0.0015p$
isolated neutrals	EM:	$\sigma(E_{isol}) = 8\%/\sqrt{E} \oplus 1.5\%$
	HAD:	$\sigma(E_{isol}) = 55\%/\sqrt{E} \oplus 12\%$
neutrals in jets	EM:	$\sigma(E_{jet}) = 5 \times \sigma(E_{isol})$
	HAD:	$\sigma(E_{jet}) = 1.2 \times \sigma(E_{isol})$

TABLE III. Efficiencies for event tags based on counting tracks with large impact parameters with a precision vertex detector.

# tracks with $b_{\rm norm} > 3$	efficiency for $H \to WW^*$	efficiency for $H \to b\bar{b}$
0	0.334	0.006
1	0.594	0.016
2	0.769	0.043
3	0.889	0.104
4	0.944	0.184
5	0.976	0.296
6	0.990	0.432
7	0.995	0.563

TABLE IV. Results from the analyses to measure the branching fractions of the Higgs boson.

	Tag Efficiencies:				
Decay Mode	4-jet B-tag	4-jet Anti-tag	6-jets	Lepton Fit	Tau fit
$H \to b\bar{b}$	5.67%	0.24%	< 0.1%	< 0.1%	< 0.01%
$H \to WW^*$	0.11%	0.23%	1.39%	1.45%	0.03%
$H \to ZZ^*$	0.07%	0.36%	0.76%	< 0.1%	0.04%
$H \to c\bar{c} + H \to gg$	3.72%	5.80%	0.75%	<0.1%	<0.1%
$H \to \tau^+\tau^-$	< 0.1%	< 0.1%	< 0.1%	0.42%	11.5%
Background(50 fb^{-1})	109.2 events	196.9 events	39.4 events	62.2 events	3 events
Signal-to-Noise	1.07:1	0.06:1	0.45:1	0.39:1	5.8:1

TABLE V. The numerical values of the errors shown in Fig. 10. The errors are calculated assuming Standard Model coupling for the Higgs and 50 fb^{-1} of integrated luminosity at $\sqrt{s}$ = 400 GeV. The errors for the 120 GeV Higgs mass assume the same signal to noise as in Table IV, except for the mode $H \to \tau^+\tau^-$, where the background was doubled to account for extra Z-pair background.

	MH = 140 GeV	MH =120 GeV
Branching Fraction	Expected error	Extrapolated Error
$\frac{\sigma(\sigma_{tot}\times\Gamma(H\to b\bar{b}))}{\sigma_{tot}\times\Gamma(H\to b\bar{b})}$	= ±12%	±7%
$\frac{\sigma(\sigma_{tot}\times\Gamma(H\to WW^*))}{\sigma_{tot}\times\Gamma(H\to WW^*)}$	= ±24%	±48%
$\frac{\sigma(\sigma_{tot}\times\Gamma(H\to c\bar{c}+gg))}{\sigma_{tot}\times\Gamma(H\to c\bar{c}+gg)}$	= ±116%	±39%
$\frac{\sigma(\sigma_{tot}\times\Gamma(H\to\tau^+\tau^-))}{\sigma_{tot}\times\Gamma(H\to\tau^+\tau^-)}$	= ±22%	±14%

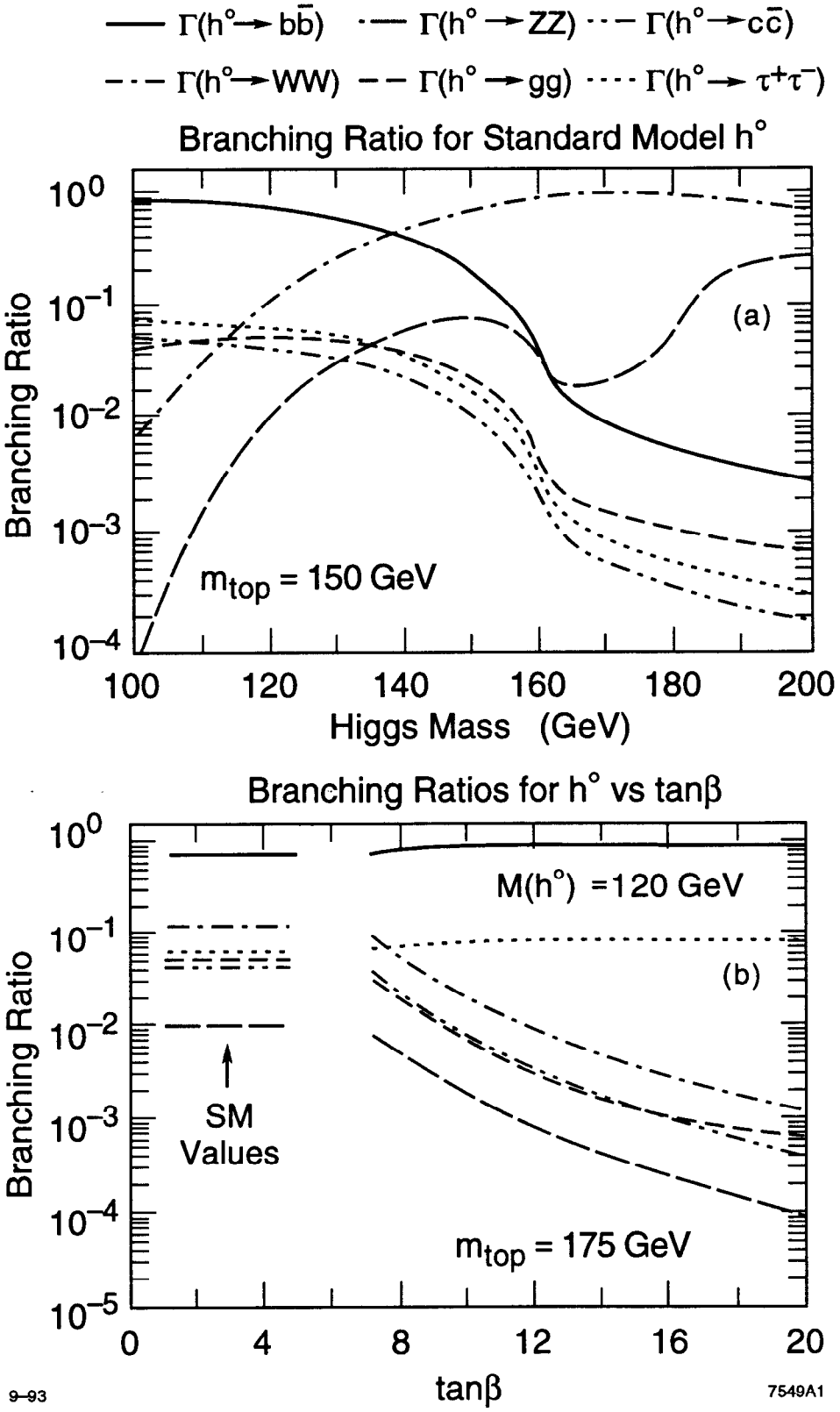
Γ(h°→bb̄)
Γ(h°→ZZ)
Γ(h°→cc̄)
Γ(h°→WW)
Γ(h°→gg)
Γ(h°→τ⁺τ⁻)
Branching Ratio for Standard Model h°
Branching Ratio
10⁰
10⁻¹
10⁻²
10⁻³
10⁻⁴
(a)
m_top = 150 GeV
100
120
140
160
180
200
Higgs Mass (GeV)
Branching Ratios for h° vs tanβ
M(h°) =120 GeV
(b)
SM
Values
m_top = 175 GeV
10⁻⁵
0
4
8
12
16
20
tanβ
9-93
7549A1

Fig. 1

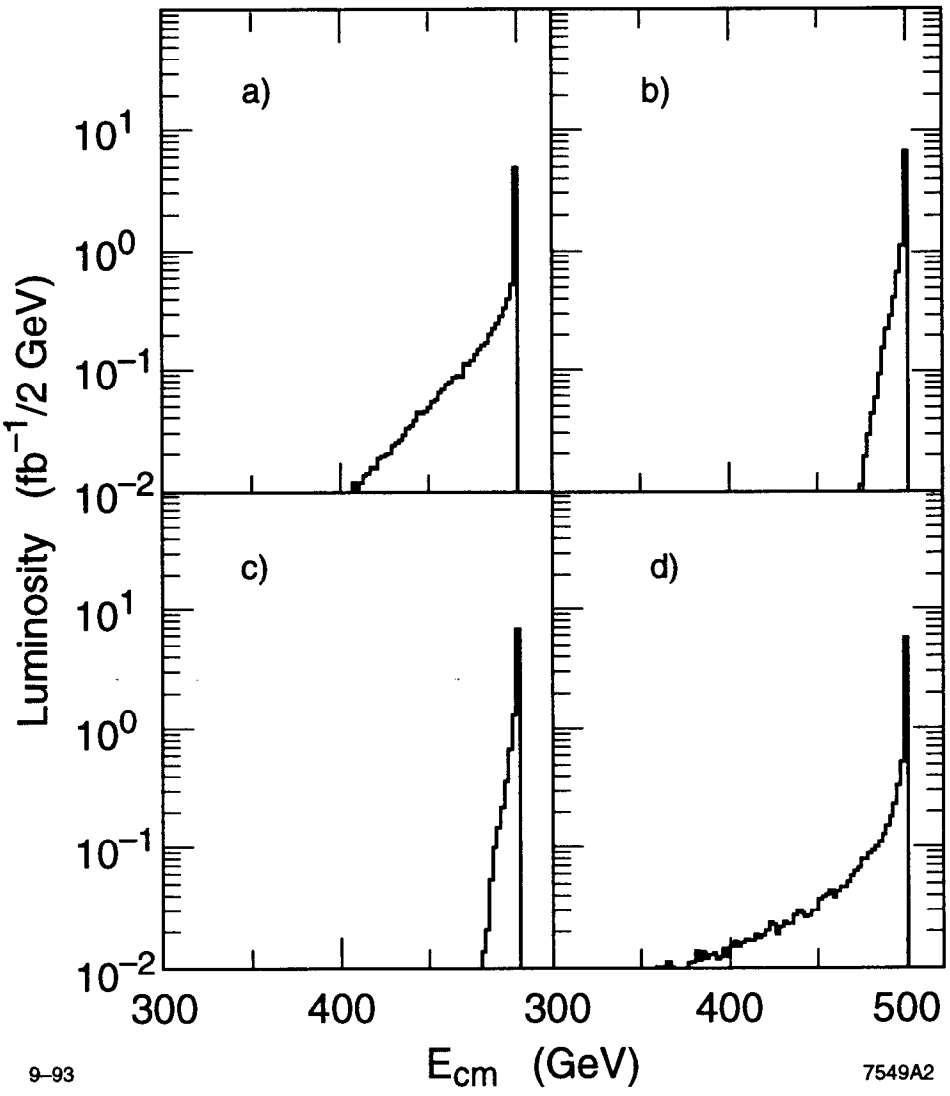
a)
b)
c)
d)
Luminosity (fb^{-1}/2 GeV)
10^{1}
10^{0}
10^{-1}
10^{-2}
300
400
300
400
500
E_{cm} (GeV)
9–93
7549A2

Fig. 2

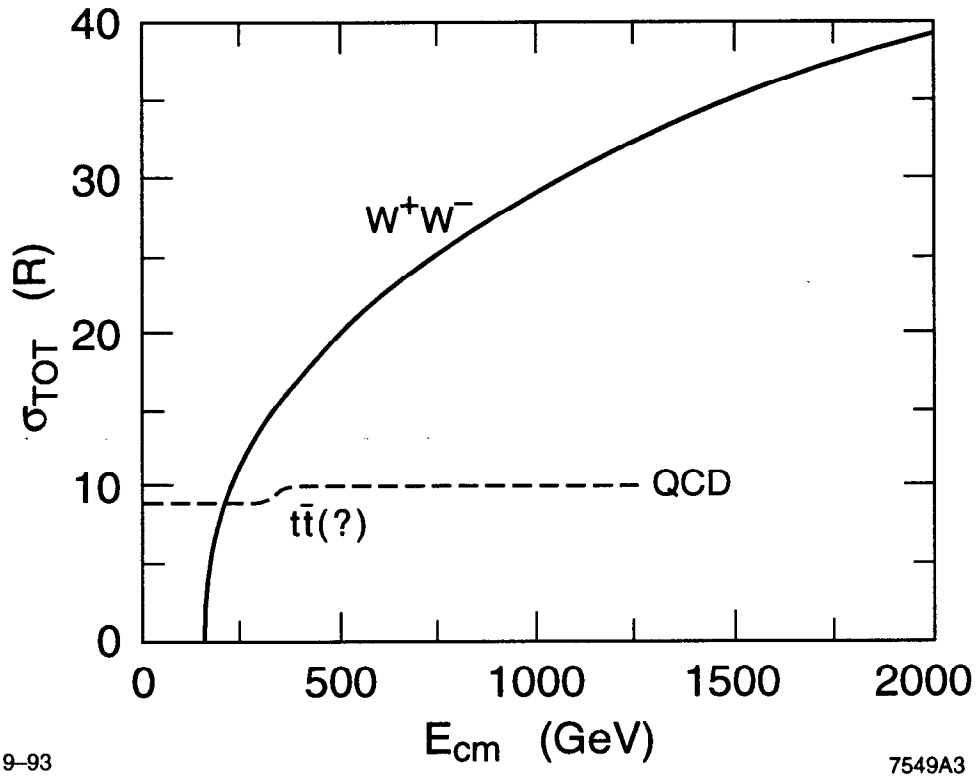
40
30
20
10
0
σ_{TOT} (R)
W^+W^-
QCD
$t\bar{t}$(?)
0
500
1000
1500
2000
E_{cm} (GeV)
9–93
7549A3

Fig. 3

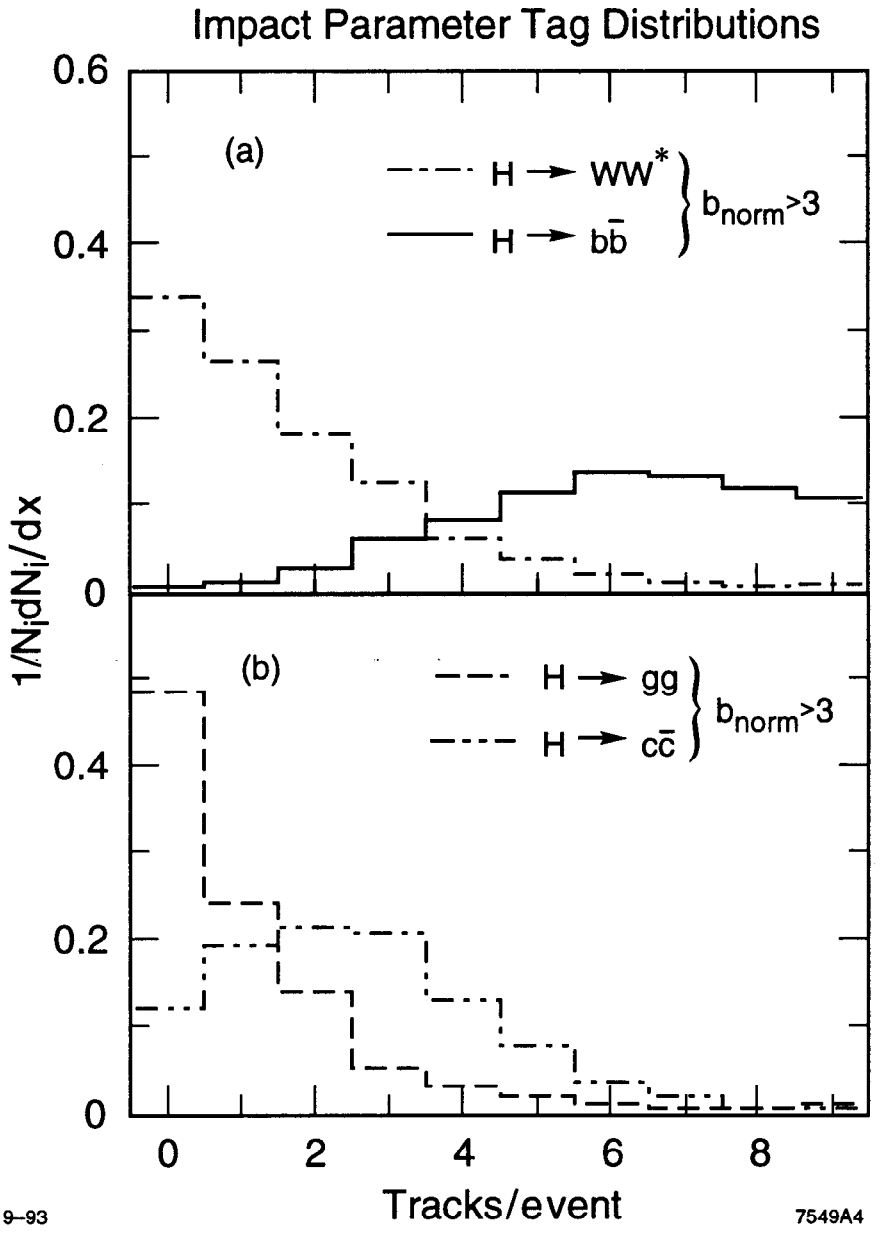
Impact Parameter Tag Distributions
0.6
0.4
0.2
0
(a)
H → WW*
H → bb̄
b_norm>3
1/N_j dN_j/dx
(b)
H → gg
H → cc̄
b_norm>3
0.4
0.2
0
0
2
4
6
8
Tracks/event
9–93
7549A4

Fig. 4

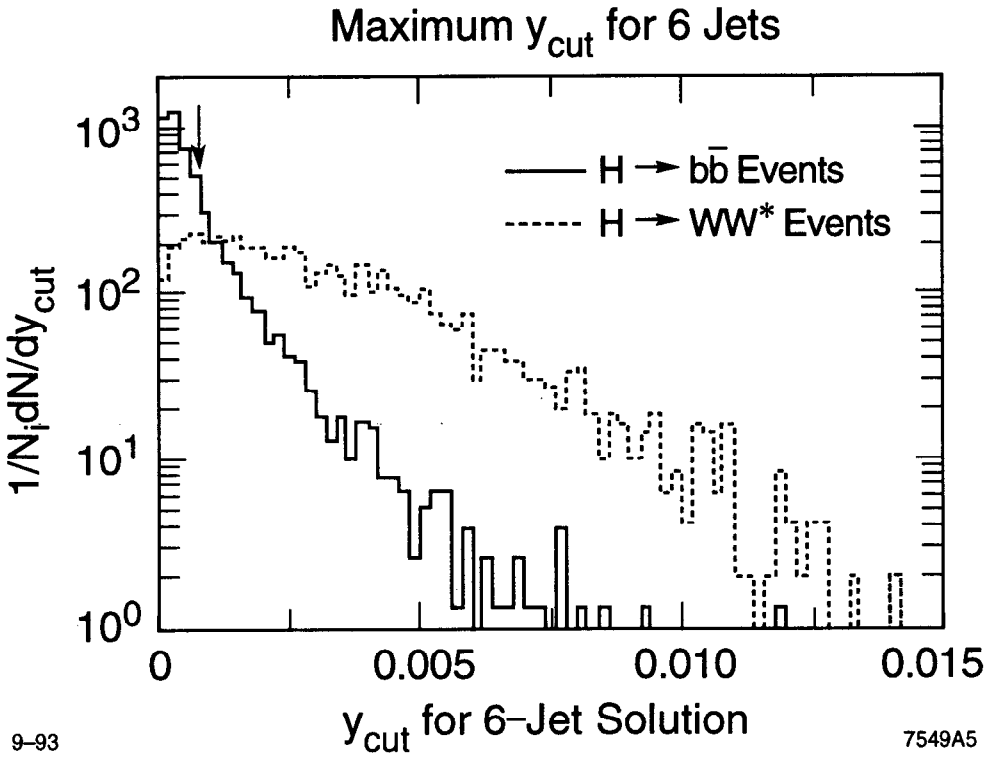
Maximum y_{cut} for 6 Jets
10^3
10^2
10^1
10^0
$1/N_j dN/dy_{cut}$
H → bb̄ Events
H → WW* Events
0
0.005
0.010
0.015
y_{cut} for 6–Jet Solution
9–93
7549A5

Fig. 5

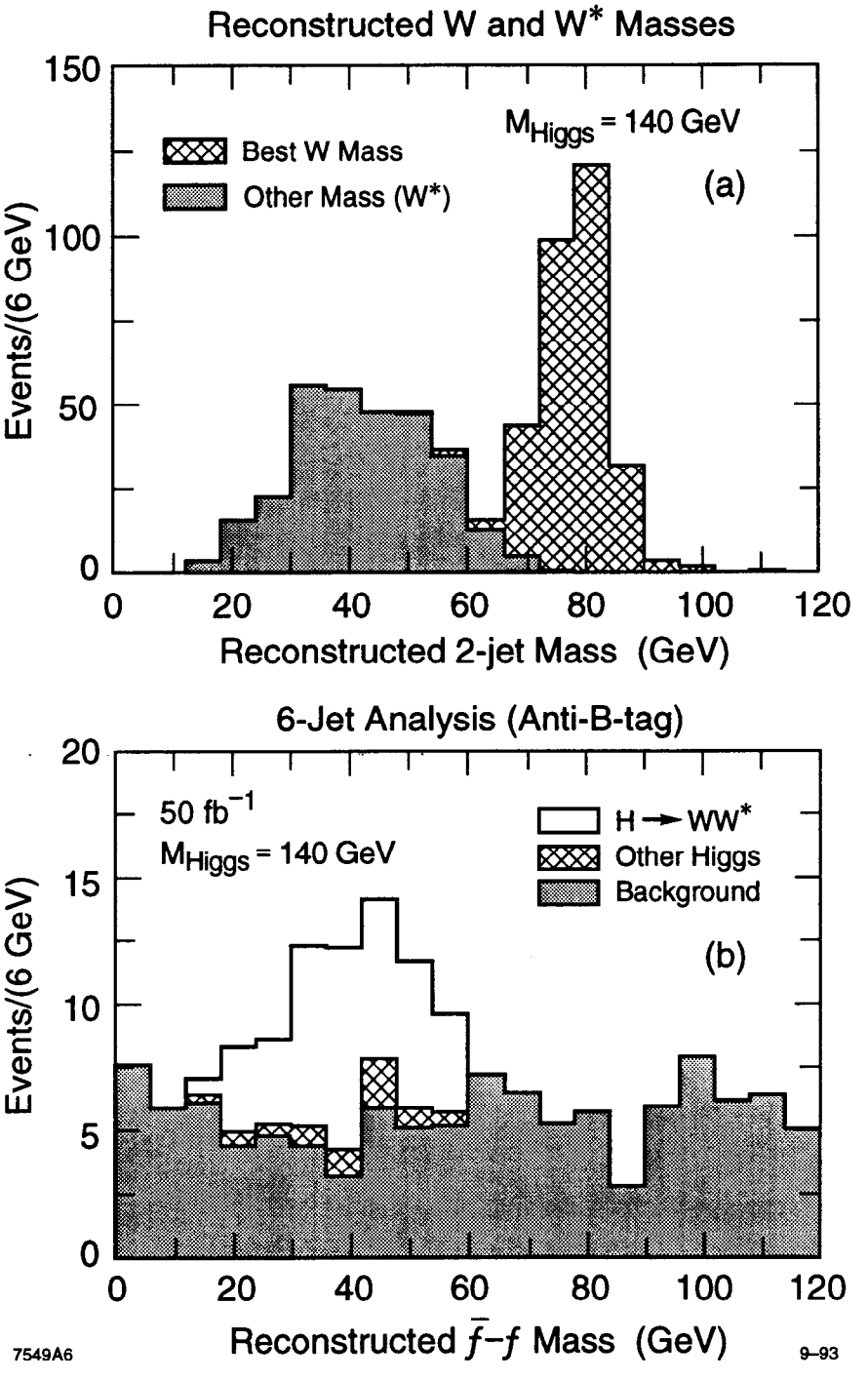
Reconstructed W and W* Masses
150
100
50
0
Events/(6 GeV)
M_{Higgs} = 140 GeV
Best W Mass
Other Mass (W*)
(a)
0
20
40
60
80
100
120
Reconstructed 2-jet Mass (GeV)
6-Jet Analysis (Anti-B-tag)
20
15
10
5
0
Events/(6 GeV)
50 fb^{-1}
M_{Higgs} = 140 GeV
H → WW*
Other Higgs
Background
(b)
0
20
40
60
80
100
120
Reconstructed $\bar{f}$–f Mass (GeV)
7549A6
9–93

Fig. 6

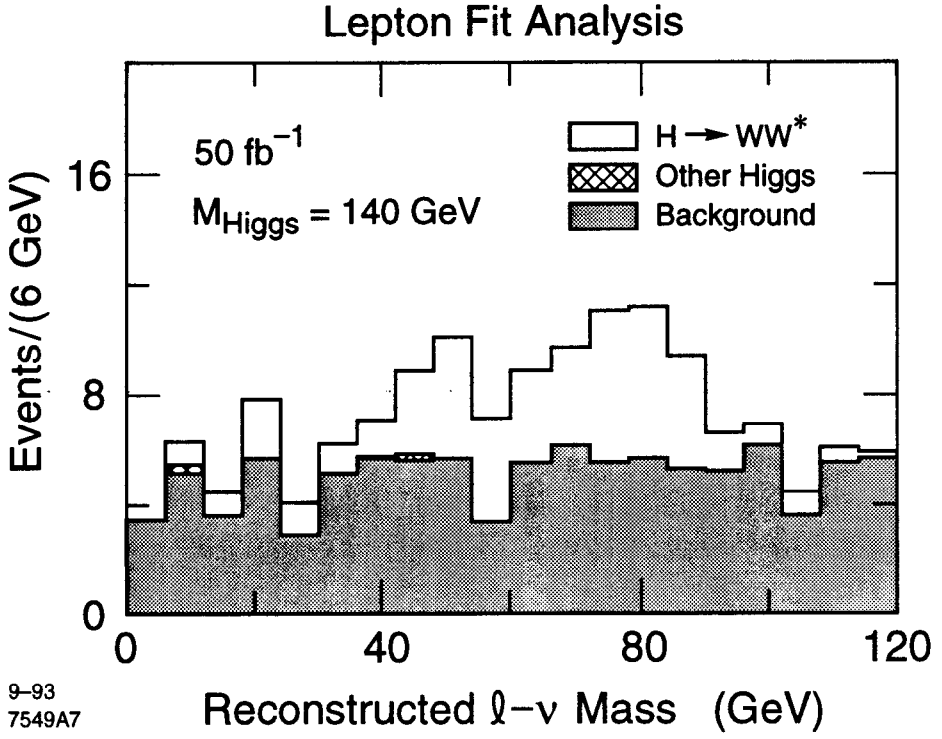
Lepton Fit Analysis
50 fb^{-1}
M_{Higgs} = 140 GeV
H → WW*
Other Higgs
Background
Events/(6 GeV)
16
8
0
0
40
80
120
Reconstructed ℓ−ν Mass (GeV)
9–93
7549A7

Fig. 7

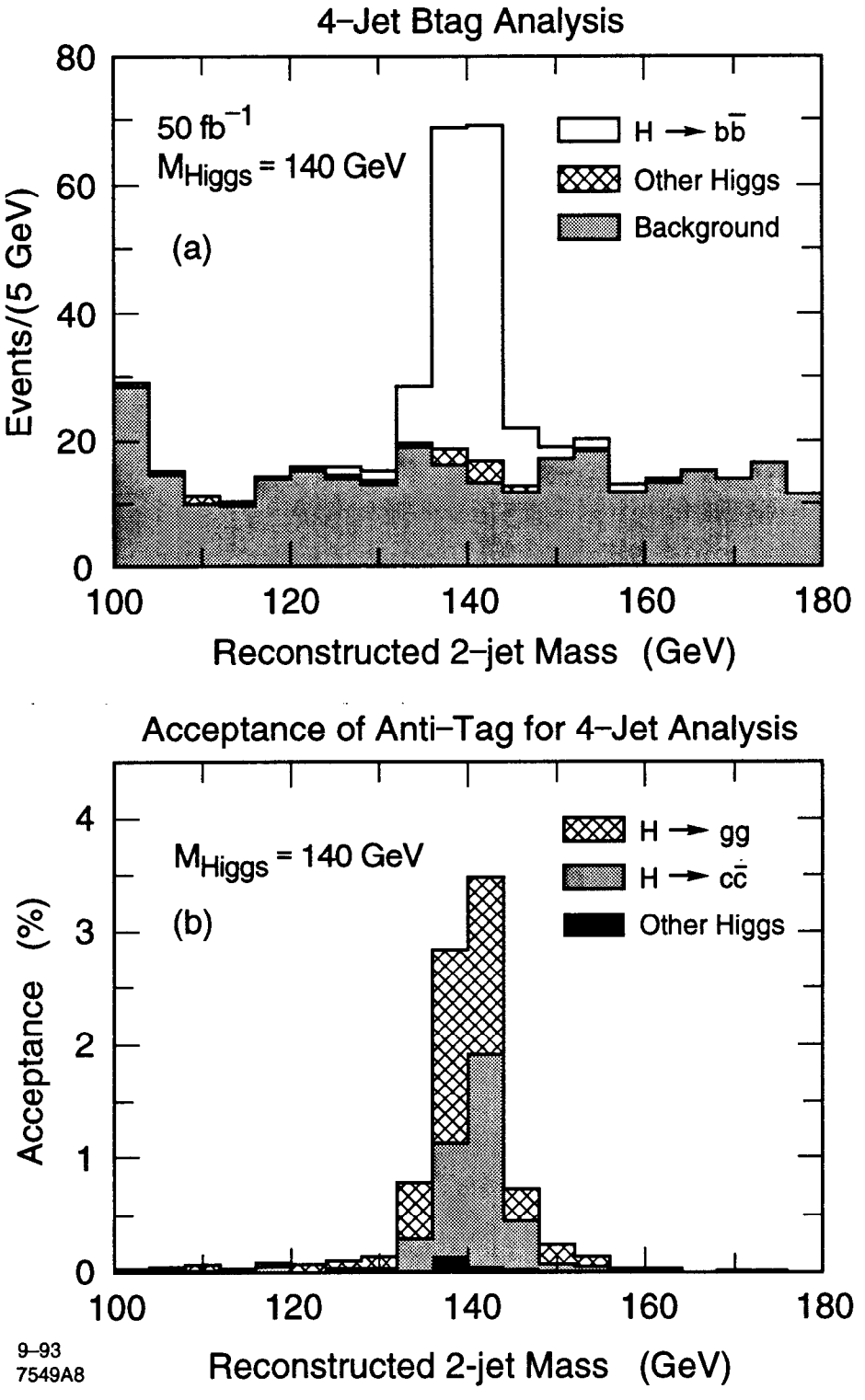
4-Jet Btag Analysis
50 fb^{-1}
M_{Higgs} = 140 GeV
(a)
H → bb̄
Other Higgs
Background
Events/(5 GeV)
Reconstructed 2-jet Mass (GeV)
Acceptance of Anti-Tag for 4-Jet Analysis
M_{Higgs} = 140 GeV
(b)
H → gg
H → cc̄
Other Higgs
Acceptance (%)
Reconstructed 2-jet Mass (GeV)
9-93
7549A8

Fig. 8

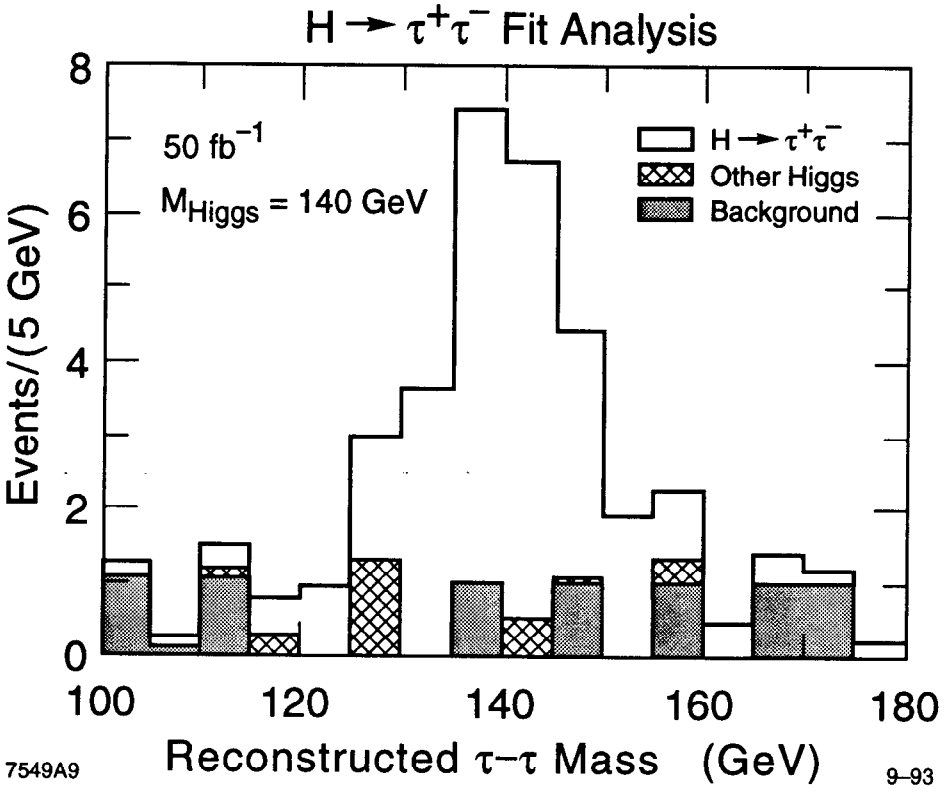
H → τ+τ− Fit Analysis
50 fb−1
MHiggs = 140 GeV
H → τ+τ−
Other Higgs
Background
Events/(5 GeV)
0
2
4
6
8
100
120
140
160
180
Reconstructed τ−τ Mass (GeV)
7549A9
9–93

Fig. 9

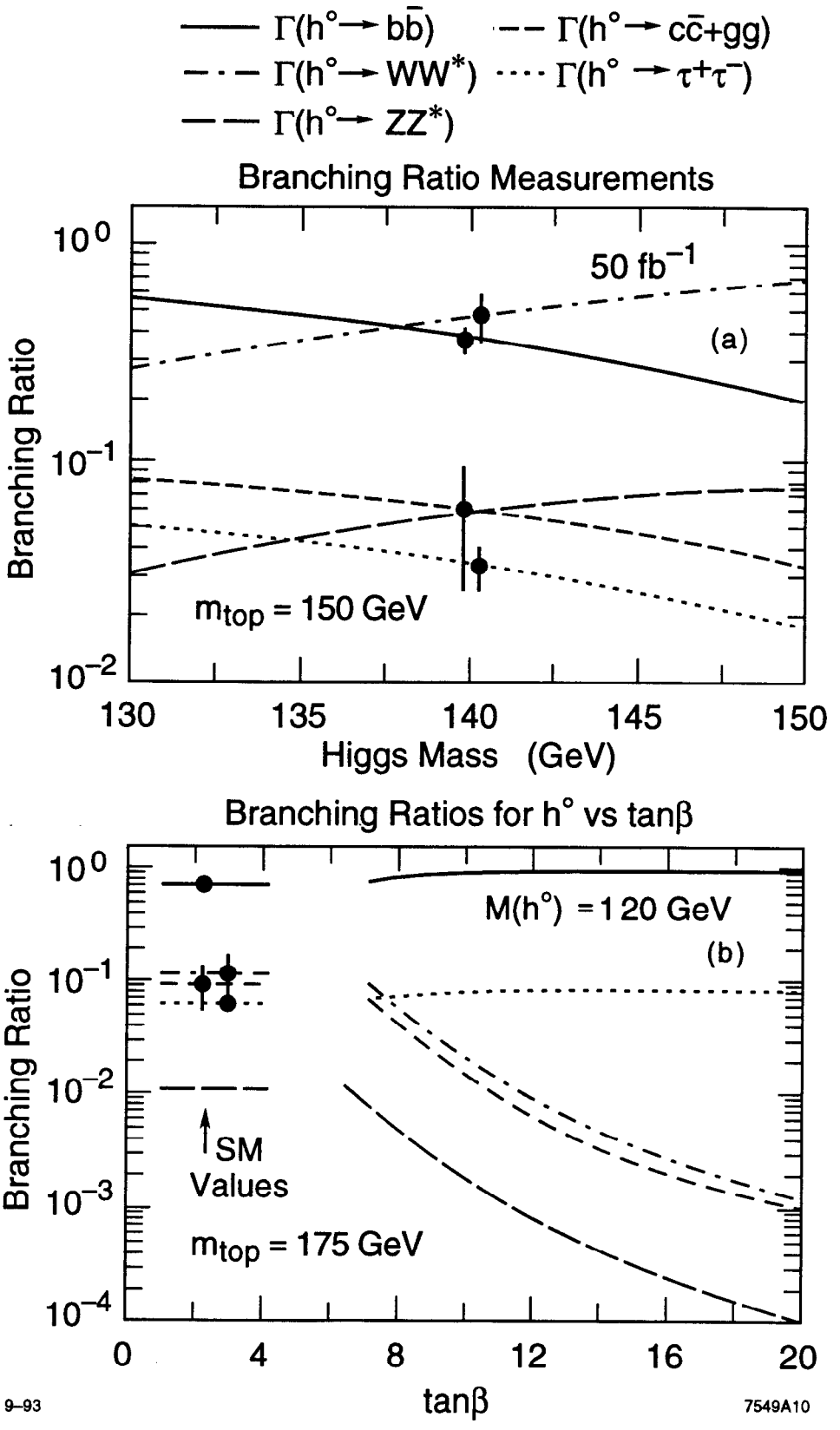
Γ(h°→ bb̄)
Γ(h°→ cc̄+gg)
Γ(h°→ WW*)
Γ(h° → τ+τ−)
Γ(h°→ ZZ*)
Branching Ratio Measurements
50 fb−1
(a)
mtop = 150 GeV
Branching Ratio
Higgs Mass (GeV)
Branching Ratios for h° vs tanβ
M(h°) = 120 GeV
(b)
SM Values
mtop = 175 GeV
tanβ
9–93
7549A10

Fig. 10